Avoidance model for soft particles. II. Positional ordering of charged rods

Eric M. Kramer* and Judith Herzfeld†
Department of Chemistry, MS 015, Brandeis University, Waltham, Massachusetts 02454-9110
(Received 5 November 1999; revised manuscript received 6 March 2000)

The phase diagram of parallel, charged spherocylinders is computed. The topology of the diagram is found to be similar to the uncharged one, but there are several qualitative changes. Regions of phase coexistence are significantly narrower and positional ordering is stabilized by the electrostatic repulsions. The nematic phase occupies a very narrow zone. We suggest that soft repulsions between surfactant micelles may be responsible for the absence of a nematic phase in most surfactant systems. We also present comparisons with the observed nematic-smectic phase transition for fd and tobacco mosaic virus particles.

PACS number(s): 82.70.Dd, 64.70.Md

I. INTRODUCTION

In this paper we consider the phase diagram of parallel, monodisperse, charged spherocylinders. We limit consideration to parallel rods because the *uncharged* system has already been well characterized, both theoretically [1,2] and in computer simulations. Stroobants, Lekkerkerker, and Frenkel [3] performed Monte Carlo simulations of parallel rods interacting via strictly hard-core repulsions. They found a surprisingly rich phase diagram. At large aspect ratios, the system exhibits the phase sequence nematic-smectic-columnar-crystalline with increasing concentration. The columnar phase becomes unstable for aspect ratios below $L/D\sim 3$ and the smectic phase becomes unstable below $L/D\sim 1$. Their results were notable because it was a convincing demonstration that the smectic phase could occur in a hard-core system, without an attractive potential.

This system has also inspired a number of theoretical investigations [1,2,4,5]. In particular, Taylor, Hentschke, and Herzfeld [1] obtained semiquantitative agreement with the results of simulations by combining a cell model for positional ordering with a scaled particle treatment of the fluid dimensions. This approach has the advantage of simplicity, and we adopt it below.

The goal of this paper is to examine the influence of soft repulsions on the phase diagram of a well-characterized model system. Soft repulsions introduce qualitative changes which should be relevant for the behavior of lyotropic liquid crystals and micellar systems. One important feature of micellar systems is the prominence of positional ordering, such that the nematic phase is either limited to a narrow range of concentrations or absent [6,7]. We shall see that this behavior may be due to soft repulsions.

The effects of soft repulsions are incorporated using the avoidance model described by Han and Herzfeld [8] and Kramer and Herzfeld [9]. A variational *avoidance diameter* is introduced to account for the density-dependent short-range order between the rods. In the first paper in this series [9], we showed that this theory provides very good agreement with the equation of state for charged spheres and reproduces the qualitative dependence of the isotropic-nematic transition of charged rods on salt concentration. Our approach has several general similarities to that of Graf and co-workers [10,11], but it differs in important details and our results disagree with theirs in some significant respects.

The paper is organized as follows. In Sec. II we present the free energy for parallel, charged spherocylinders. The avoidance model for soft particles and the cell model for positional ordering are briefly reviewed. Our results are presented in Sec. III. We discuss the dependence of the phase diagram on particle aspect ratio and ionic strength, and make a comparison to the nematic-smectic transition of fd and tobacco mosaic (TMV) virus particles. The paper is concluded in Sec. IV.

II. THE MODEL

A. The avoidance model for soft rods

Consider a monodisperse fluid of N spherocylinders in a volume V at temperature T. The spherocylinders have a cylindrical length L and a hard-core diameter D_0. There are also soft repulsions between the particles, which produce short-range order. The avoidance model approximates this short-range order by assuming (1) an exclusionary zone around each particle that extends to an ''avoidance diameter'' $D_a \geq D_0$ and (2) a flat particle distribution beyond. The result is that the excess free energy is divided into an entropic piece and an energetic piece. Increasing the avoidance diameter decreases the energetic contribution and increases the entropic contribution. The trade-off between the two defines a minimum free energy corresponding to an avoidance diameter that approximates the equilibrium short-range order of the particles.

The entropic contribution to the free energy F_S is approximated by the configuration integral for hard-core spherocylinders of the same length and number density, but with a diameter D_a. The energetic part of the free energy F_U is due to the mean field of all particles outside the avoidance volume. For rods, we approximate this contribution by dividing each rod into τ segments with a pair correlation function

$$\zeta(r)=n\tau g(r), \quad g(r)=\begin{cases}0, & r<D_a\\ 1 & r>D_a,\end{cases} \tag{1}$$

*Present address: Physics Department, Simons Rock College, Great Barrington, MA 01230.
†Author to whom correspondence should be addressed. Electronic address: herzfeld@brandeis.edu

and pairwise potential

$$\tilde{u}(r)=\begin{cases}\infty, & r<D_a\\ u(r)=\beta U(r), & r>D_a,\end{cases} \tag{2}$$

where $\beta=1/kT$, and $U(r)>0$ is the soft part of the repulsive potential. The choice of an isotropic correlation function may seem excessively crude for an application to parallel charged rods since (1) it does not give special treatment to charges located on the same rod and (2) it does not include the expected correlation between neighboring rods due to positional ordering. However, it was previously found that a large change in $\zeta(r)$ had a relatively small effect on the resulting phase diagrams [9,12]. We make the isotropy assumption for simplicity and for consistency with the previous paper in this series, Ref. [9]. The reader is referred there for a more thorough discussion of the adequacy of the approximation.

The equilibrium value of the total Helmholtz free energy is determined by minimizing with respect to D_a,

$$F=\min_{D_a}(F_I+F_S+F_U). \tag{3}$$

The first term is the ideal gas contribution

$$\frac{\beta F_I[T,V,N]}{N}=\ln(n\Lambda^3)-1, \tag{4}$$

where $\beta=1/k_BT$, $n=N/V$ is the number density of spherocylinders, and $\Lambda=(\beta h^2/2\pi m)^{1/2}$ is the thermal wavelength of one spherocylinder. The second term is the phase-dependent configuration integral for parallel spherocylinders with hard-core diameter D_a. This is calculated in the next section, using the model of Taylor, Hentschke, and Herzfeld [1]. The third term is the energetic contribution

$$\frac{\beta F_U[T,V,N;D_a]}{N}=\tfrac{1}{2}\tau\int d\mathbf{r}\,u(\mathbf{r})\zeta(\mathbf{r})$$
$$=2\pi\tau^2 n\int_{D_a}^{\infty}dr\,r^2u(r). \tag{5}$$

The minimization in Eq. (3) is done numerically with a downhill simplex minimization routine [13].

B. Configuration integral

For the configurational entropy of parallel spherocylinders, we use the expressions derived in Refs. [1] and [2], based on the combination of a cell model for the positionally ordered dimensions and scaled particle theory for the fluid dimensions. For example, the layered structure of the smectic phase is imposed by an infinite array of parallel walls. The configuration integral of the rods then factors into a piece due to the one-dimensional crystalline order perpendicular to the walls and the two-dimensional fluid order parallel to the walls. The term due to crystalline order is a straightforward phase space calculation, and the fluid term is approximated using two-dimensional scaled particle theory. The use of walls to enforce positional ordering exaggerates the degree of order in the system and forces all phase transitions to be first order. Its chief advantage is that it allows a calculation of the free energy in closed form for each phase. We adopt the expressions of Ref. [1] with the following change: the avoidance diameter D_a is substituted for the bare spherocylinder diameter D_0.

In the nematic phase there is no positional ordering and

$$\frac{\beta F_S[T,V,N;D_a]}{N}=-\ln(1-\phi_a)+3\frac{\phi_a}{1-\phi_a}$$
$$+\frac{C}{3}\left(\frac{\phi_a}{1-\phi_a}\right)^2\quad\text{(nematic)}, \tag{6}$$

where $C=\gamma(D_a+2L)$, $\gamma=(L+D_a)/(L+2D_a/3)^2$, and $\phi_a=n(\pi D_a^3/6+\pi D_a^2L/4)$ is the particle volume fraction.

In the smectic phase, the volume is partitioned into layers by planar walls oriented perpendicular to the spherocylinders. The walls are spaced Δ_s apart. It is required that $L+D_a\leqslant\Delta_s\leqslant 2(L+D_a)$ to ensure that a layer can accommodate the length of one and only one spherocylinder. The free energy is

$$\frac{\beta F_S[T,V,N;D_a,\Delta_s]}{N}=-\ln\left(1-\frac{D_a+L}{\Delta_s}\right)-\ln(1-\phi_2)$$
$$+\frac{\phi_2}{1-\phi_2}\quad\text{(smectic)}, \tag{7}$$

where $\phi_2=\phi_a\gamma\Delta_s/(D_a+L)$ is the fractional area occupied by the spherocylinders in a layer. The smectic layer spacing found by minimizing the free energy with respect to Δ_s is

$$\frac{\Delta_s}{D_a+L}=\frac{9}{8h}\{1-2\sin[\tfrac{1}{3}\arcsin(1-h)]\}, \tag{8}$$

where $h=27\phi_a\gamma/16$ and the arcsine is defined to have the range $[-\pi/2,\pi/2]$.

In the columnar phase the volume is partitioned into close-packed columns of hexagonal cross section oriented parallel to the spherocylinders. The short diameter of the hexagon is Δ_c. It is required that $D_a\leqslant\Delta_c\leqslant 2D_a$ to ensure that a column can accommodate the width of one and only one spherocylinder. The free energy (after minimization with respect to Δ_c) is

$$\frac{\beta F_S[T,V,N;D_a]}{N}=-3\ln\left(1-\frac{D_a}{\Delta_c}\right)\quad\text{(columnar)}, \tag{9}$$

with

$$\frac{\Delta_c}{D_a}=\left(\frac{2\sqrt{3}}{\pi}\gamma\phi_a\right)^{1/3}. \tag{10}$$

In the crystalline phase, there is one particle per cell. Each cell is a hexagonal tube of length Θ and short diameter Δ_x, capped at each end by half a rhombic dodecahedron. When $\Theta=0$, this reduces to a space-filling packing of rhombic dodecahedrons. Minimization of the free energy with respect to Θ gives $\Theta/\Delta_x=L/D_a$. Minimization with respect to Δ_x gives $\Delta_x=D_a(\phi_a/\phi_a^{\rm cp})^{1/3}$ and the free energy

$$\frac{\beta F_S[T,V,N;D_a]}{N} = 1 - 3\ln\left[1 - \left(\frac{\phi_a}{\phi_a^{\rm cp}}\right)^{1/3}\right] \quad \text{(crystalline)}, \tag{11}$$

where $\phi_a^{\rm cp}$ is the close-packed volume fraction of parallel spherocylinders,

$$\phi_{\rm CP} = \frac{\pi}{3\sqrt{2}} \frac{(D_a + \frac{3}{2}L)}{(D_a + (\sqrt{3/2})L)}. \tag{12}$$

C. Choice for the potential *u*

In this paper we are mainly interested in the effects of electrostatic repulsions on the phase diagram. We therefore assume a net charge Qe is distributed evenly along the cylinder axis, where e is the proton charge. The charge per unit length is $\nu = Qe/L$. For calculations in which we divide the charge among τ segments, the charge per segment is $qe = Qe/\tau$.

The electrostatic repulsion between polyions depends on the ionic strength of the solution, $I = \frac{1}{2}\Sigma Z_i^2 n_i$ where n_i and Z_i are the concentration and valence of species i and the sum is over all species except the polyions. The two length scales characterizing the electrostatic repulsion are the Bjerrum length $\xi_B = \beta e^2/\epsilon$, where ϵ is the dielectric constant of the solvent, and the Debye-Huckel decay length $\lambda = (8\pi\xi_B I)^{-1/2}$. In water at 300 K, $\epsilon = 78$, $\xi_B = 7.1$ Å, and $\lambda = (3.0\,\text{Å})/\sqrt{I}$ where I has units of molarity.

The Debye-Huckel expression for the electrostatic potential between two point charges is $u(r) = \beta U(r) = q^2(\xi_B/r)e^{-r/\lambda}$. For this potential, Eq. (5) may be integrated to give

$$\frac{\beta F_U}{N} = 2\pi Q^2 n \xi_B \lambda^2 \left(1 + \frac{D_a}{\lambda}\right) e^{-D_a/\lambda}. \tag{13}$$

Debye-Huckel theory is only valid for weakly charged systems, such that the potential energy of an ion in solution does not exceed kT. For higher charge, one must include the nonlinear effects contained in the Poisson-Boltzmann (PB) equation [14]. We account for the nonlinear effects using Manning's theory of counterion condensation [15]. In its simplest form, condensation theory ignores the details of the counterion distribution near the rod and assumes that a fraction of the charge on the rod will be neutralized due to nonspecific binding with counterions. For a salt solution in which the counterions have valence Z_c, the *effective* linear charge density on a rod is predicted to be

$$\nu_{\rm eff} = \text{sgn}(\nu)\min\left(|\nu|, \frac{e}{|Z_c|\xi_B}\right). \tag{14}$$

The Debye-Huckel expression for the interparticle potential may then be used without change, but is only strictly valid for distances greater than about λ from the surface of the cylinder [14]. Charge condensation thus sets an approximate upper bound on our choice for ν, or equivalently on Q. Most of the published experiments on viruses use a monovalent counterion, so we use $|\nu_{\rm eff}| \leq e/\xi_B$.

In addition to the nonlinear PB effects, described adequately by Manning's theory, there has been much recent research into possible attractive interactions between like-charged colloids [16]. Although the mechanism is still under debate, most proposals describe a short-range force ($<\lambda$) which increases in magnitude with the valence of the counterions Z. If attractive forces play a prominent role, then a different potential u should be used and the resulting F_U will be significantly lower. In the experiments we discuss below, monovalent counterions were used and attractions are not expected to be significant.

D. Phase coexistence

The conditions for phase coexistence are equality of pressures and chemical potentials. The pressures in the nematic, smectic, columnar, and crystalline phases are, respectively,

$$\frac{\beta p}{n} = \frac{1}{1-\phi_a}\left[1 + 3\left(\frac{\phi_a}{1-\phi_a}\right) + 2C\left(\frac{\phi_a}{1-\phi_a}\right)^2\right] + \frac{\beta F_U}{N} \quad \text{(nematic)}, \tag{15}$$

$$\frac{\beta p}{n} = \frac{1}{(1-\phi_2)^2} + \frac{\beta F_U}{N} \quad \text{(smectic)}, \tag{16}$$

$$\frac{\beta p}{n} = \frac{1}{(1-D/\Delta_c)} + \frac{\beta F_U}{N} \quad \text{(columnar)}, \tag{17}$$

$$\frac{\beta p}{n} = \frac{1}{(1-D/\Delta_x)} + \frac{\beta F_U}{N} \quad \text{(crystalline)}, \tag{18}$$

and in all cases the chemical potential per spherocylinder is

$$\beta\mu = \frac{\beta p}{n} + \frac{\beta F}{N}. \tag{19}$$

III. RESULTS

In this paper we use parameter values suggested by experiments on virus particles in water [17]. The virus fd has a bare diameter $D_0 = 66$ Å and length $L = 8800$ Å, with aspect ratio 133. The fd particles are semiflexible, with a persistence length about $3L$, so the rigid spherocylinders considered here should be a fair model. Tobacco mosaic virus particles have a bare diameter $D_0 = 180$ Å and length $L = 3000$ Å, with aspect ratio 16.7. TMV particles are inflexible for most practical purposes. Particles of both viruses are highly charged at $p\text{H} > 7$, with a linear charge density $\nu \geq -(1-2)e/\text{Å}$. Including the effects of counterion condensation [15] leads to an effective linear charge density $\nu_{\rm eff} = -e/(7.1\,\text{Å})$. This gives $Q = 1240$ for fd and 422 for TMV.

Figure 1 shows the dependence of D_a on particle volume fraction for a moderate $\nu = -0.07e/\text{Å}$ (about half of the effective charge density of the virus particles). We see that the avoidance diameter increases with aspect ratio and generally decreases with increasing volume fraction. This is due to the greater entropic cost of avoidance for shorter particles and higher volume fractions. An exception to the latter trend occurs at the phase transitions. There, an increase in free volume due to particle alignment decreases the entropic cost of avoidance.

Figure 2 shows the cell model results for the phase dia-

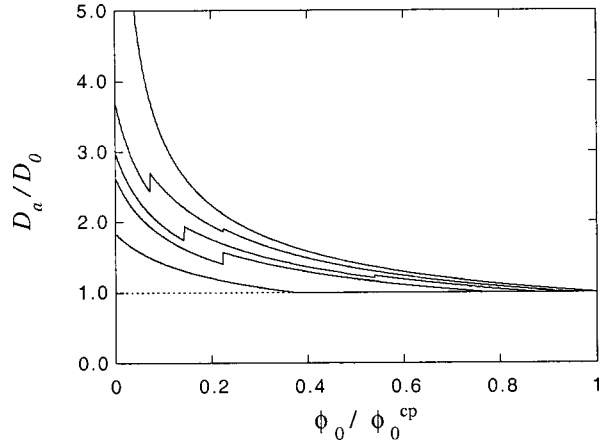

FIG. 1. Avoidance diameter vs solute volume fraction for five values of the spherocylinder aspect ratio. The dashed line at the top is for $L/D_0=\infty$. The four solid lines are for (bottom to top) $L/D_0=3$, 7, 10, and 20. The effective linear charge density is $\nu=-0.07\,e/\text{Å}$ and the bare diameter is $D_0=66\,\text{Å}$. The Debye-Huckel decay length is $\lambda=D_0=66\,\text{Å}$, corresponding to an ionic strength of $I=2.1\,\text{m}M$. Discontinuities occur at each phase transition. Volume fractions have been normalized to the close-packing volume fraction ϕ_0^{cp} defined as in Eq. (12) with $D_a=D_0$.

gram of parallel, uncharged spherocylinders. This diagram was first calculated by Taylor, Hentschke, and Herzfeld [1]. (The phase boundaries have been shifted by ~1%, correcting a small error in the original numerical solution of Ref. [1].) The isotropic-nematic phase boundary for uncharged spherocylinders with orientational freedom, calculated using scaled particle theory [18], has been superimposed to provide a qualitative picture of the entire phase diagram of hard, rod-shaped particles.

Figure 3 shows the dramatic changes resulting from a moderate charge density on the spherocylinders ($\nu=-0.07e/\text{Å}$ as in Fig. 1). The effects are more pronounced for larger aspect ratios, which in this plot correspond to higher total charge per particle. Although the phase transitions remain first order, all coexistence regions become very narrow. We also see that, although the topology of the dia-

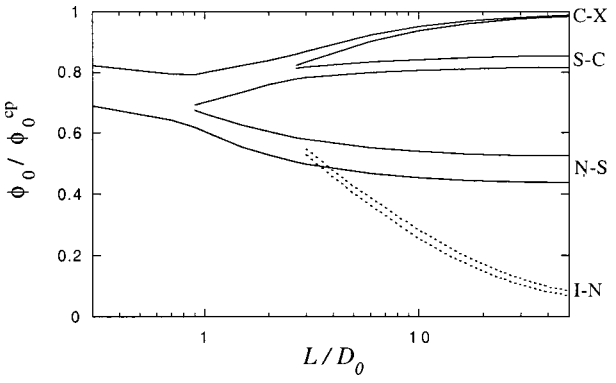

FIG. 2. Coexistence volume fractions vs aspect ratio for uncharged spherocylinders. The predictions for the positional ordering transitions (solid lines) were calculated following the approximations of Ref. [1] and the prediction for the isotropic-nematic transition (dashed lines) is derived from scaled particle theory [18]. I = isotropic phase, N = nematic phase, S = smectic phase, C = columnar phase, and X = crystalline phase.

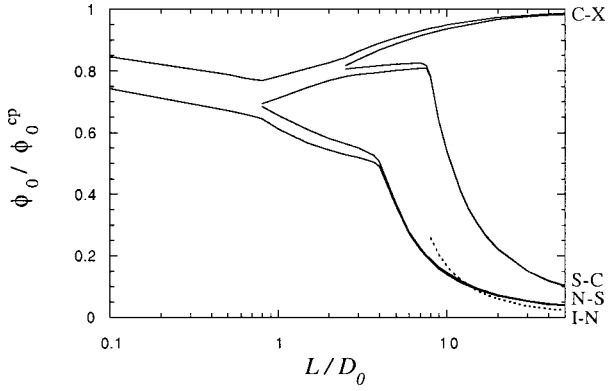

FIG. 3. Same as Fig. 2, but for charged spherocylinders with bare diameter $D_0=66\,\text{Å}$, effective linear charge density $\nu=-0.07\,e/\text{Å}$, and Debye-Huckel decay length $\lambda=D_0=66\,\text{Å}$ (the same parameter values used in Fig. 1). The predictions for the positional ordering transitions (solid lines) are from the present work and the prediction for the isotropic-nematic transition (dashed lines) is from Kramer and Herzfeld [9].

gram has not changed, charge tends to stabilize the positionally ordered phases, especially the columnar phase, which occupies most of the phase diagram for $L/D_0>20$.

The approximations used have the following effects on the phase diagram. (1) The use of impenetrable walls to enforce positional ordering leads to an underestimate for the configurational entropy (and hence the stability) of positionally ordered phases. This tends to raise the coexistence volume fractions. (2) As we have noted previously, the avoidance model tends to overestimate the energy of repulsions at low concentrations (see Ref. [9]). This gives an overestimate for the avoidance volume fractions at low concentrations, and thus tends to lower the coexistence volume fractions.

As found previously for the isotropic-nematic (I-N) transition [9], there is a prominent elbow in the coexistence curves. The elbow is due to the abrupt change in the slope of the free energy when D_a decreases to its limiting value of D_0. It is presumably an artifact of the use of a step function [Eq. (1)] for the pair correlation in the avoidance model.

Figure 4 shows the phase diagram calculated as in Fig. 3, but with the smectic phase removed. This is informative since small amounts of length polydispersity can destabilize

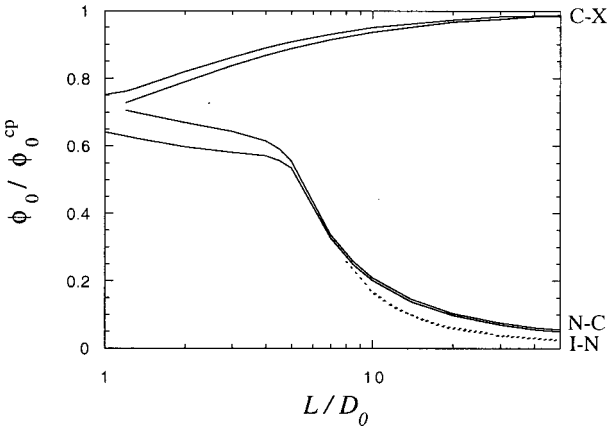

FIG. 4. Same as Fig. 3, but with the smectic phase suppressed to approximate the effect of length polydispersity.

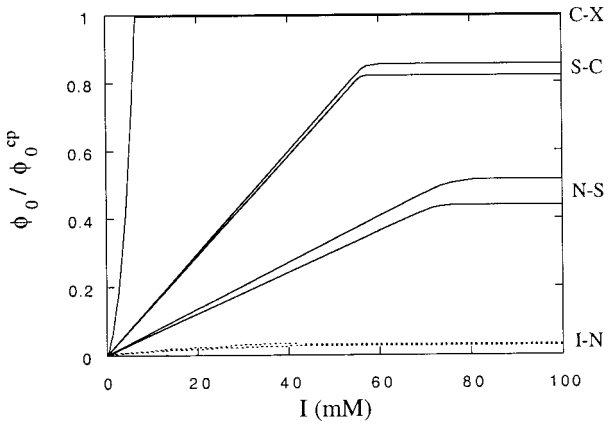

FIG. 5. Ionic strength dependence of the ordering transitions for fd virus particles. Shown are avoidance model predictions from the present work for positional ordering (solid lines) and from Kramer and Herzfeld [9] for orientational ordering (dashed lines). Parameter values appropriate for fd virus particles: aspect ratio $L/D_0 = 133$ and effective linear charge density $\nu_{\text{eff}} = -e/(7.1\ \text{Å})$. Volume fractions have been normalized to the close-packing value, $\phi_{\text{CP}} = 0.906$.

the smectic phase in real systems. In comparison with the uncharged case (Fig. 2), the region occupied by the nematic phase in Figs. 3 and 4 is extremely narrow.

Figures 5 and 6 show the phase diagram versus ionic strength for particles having the aspect ratio and linear charge density of fd virus particles. Figure 6 provides a comparison with experimental data for the isotropic-cholesteric [19] and cholesteric-smectic phase transitions [20] of fd virus particles. The fd virus particles exhibit a cholesteric phase rather than a nematic phase, but the difference in free energies due to twist is expected to be very small [19,21]. The predicted nematic-smectic (N-S) coexistence volume fractions show good agreement with the experimental data at low ionic strengths where electrostatic repulsions dominate. However, the theory significantly overestimates the transition density at high ionic strengths, where charges are well screened. This is in contrast to the good agreement between

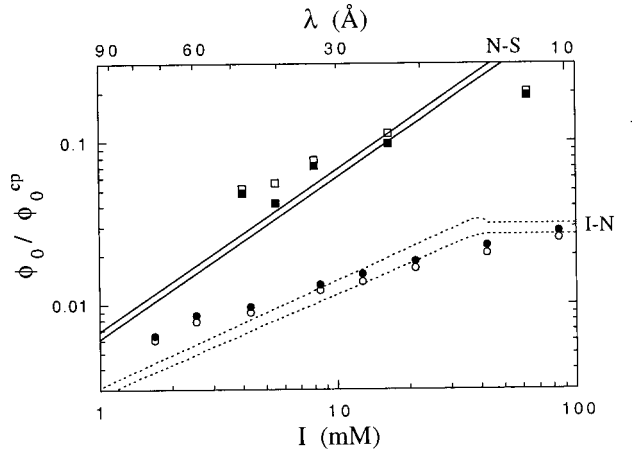

FIG. 6. Comparison of theory and experiment for the phase boundaries of fd virus particles. The theory is the same as in Fig. 5. Data are from Tang and Fraden [19] for the isotropic-cholesteric phase transition (circles) and from Dogic and Fraden [20] for the cholesteric-smectic phase transition (squares). The Debye-Huckel decay length is shown on the axis at the top.

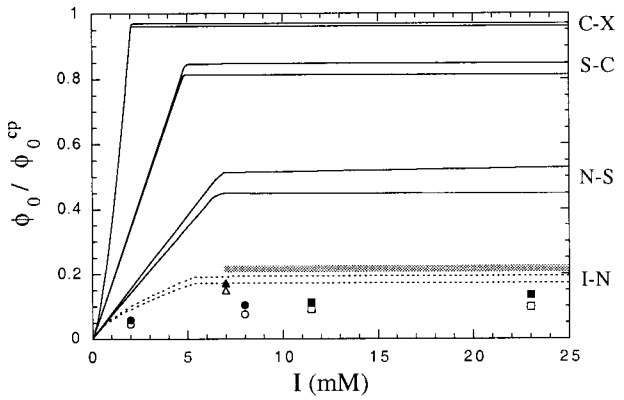

FIG. 7. Ionic strength dependence of the ordering transitions for TMV particles. Shown are avoidance model predictions from the present work for positional ordering (solid lines) and from Kramer and Herzfeld [9] for orientational ordering (dashed lines). Parameter values chosen for TMV particles: aspect ratio $L/D_0 = 17$ and dimensionless linear charge density $\nu_{\text{eff}} = -e/(7.1\ \text{Å})$. Gray bar: the region of nematic-smectic phase coexistence observed for TMV by Wen, Meyer, and Caspar [22] and Hirai *et al.* [23]. Symbols: isotropic-nematic coexistence data from Fraden Maret, and Caspar [24] for pH 7.2 (squares), pH 8.0 (circles) and pH 8.5 (triangles). Volume fractions have been normalized to the close-packing value $\phi_0^{\text{cp}} = 0.899$.

theory and experiment for the I-N transition [9]. The discrepancy in the N-S transition is therefore probably due to the tendency of the cell model to overestimate the coexistence concentrations for positional ordering of hard rods [1].

Figure 7 shows the phase diagram versus ionic strength predicted for TMV virus particles. Limited experimental data are available for the location of the nematic-smectic transition in TMV. Wen, Meyer, and Caspar [22] were able to bound the coexistence concentration between 156 and 175 mg/ml in 50m*M* Na borate at pH 8.5 ($I = 7$ m*M*). Hirai *et al.* [23] observed coexisting nematic and smectic phases at 171 mg/ml in 10m*M* Na phosphate at pH 7.2 ($I = 23$m*M*). From this we conclude that 7 m*M* is already the high salt concentration limit, and that there is no significant variation in the phase boundary for higher ionic strength. The inferred experimental phase boundary is shown as a gray bar in Fig. 7. Theory and experiment both show no significant variation in the phase boundary beyond an ionic strength of 7 m*M*. However, the experimental N-S boundary occurs at about half of the density predicted by theory. As we found for fd, the agreement is better for the I-N transition [9,24], suggesting again that it is the tendency of the cell model to overestimate the concentrations for positional ordering of hard rods that is responsible for the greater discrepancy in the N-S transition.

Overall, the agreement between theory and experiment is worse for TMV than for fd. In particular, both of the ordering transitions in TMV solutions are generally observed at lower densities than predicted by the avoidance model. This extends to the high ionic strength limit where electrostatic interactions are fully screened and the model reduces to a hard particle model. The discrepancy is still greater when the experimental data are compared to Brownian dynamics simulations of the *I-N* transition of TMV [25]. These disparities between theory and experiment could be related to the tendency of TMV particles to form end-to-end aggregates [26–28]. Such aggregation will increase the length of the

particles severalfold and thereby shift the ordering transitions to lower density. The aggregation is less when electrostatic repulsions are stronger (i.e., at low ionic strengths and/or high pH's [27] and the concentration is lower. As seen in Fig. 7, this is also where theory and experiment are in closer agreement. Aggregation would also tend to increase polydispersity and thereby destabilize the smectic phase relative to the columnar phase. In fact, order transverse to the particle axes has been observed by a number of workers [23,24,29], and the reported transverse periodicities of 300 Å in one case [23] and 460 Å in another [29] are in the range of expected columnar spacings in the avoidance model. It has also been observed that the narrowness of the smectic region in TMV may be due to aggregation [22], and that the smectic phase is more stable over time, and shows sharper reflections, for a special strain of TMV that has less tendency to aggregate [26].

It is interesting to contrast our results with those of Graf and Lowen [11], who calculated the phase diagram of charged spherocylinders with orientational freedom. The most prominent difference is their prediction of a large region of nematic stability at low ionic strengths, leading to a reentrant nematic phase below $I = 3\ \mathrm{m}M$ (compare to Figs. 5 and 7). The difference may be an artifact of the approximations they use. Conspicuous among these are (1) their assumption of a Maier-Saupe form for the orientation distribution function in all phases, including the positionally ordered phases, (2) the insensitivity of their ''effective particle diameter'' to packing constraints, (3) their *ad hoc* addition of a negative constant ($-2.25kT$ per particle) to the free energy of the nematic phase, and (4) the omission of the columnar phase from their calculations.

IV. CONCLUSIONS

In this paper we use the avoidance model for soft repulsions to extend an earlier model for the phases of parallel spherocylinders. This provides a further test for the utility of the avoidance model developed in Refs. [8] and [9]. It is also used to calculate the phase diagram of parallel charged spherocylinders.

Comparison with the nematic-smectic phase transition of fd virus particles shows good agreement under conditions where electrostatic repulsions are important. On the other hand, at high ionic strengths, the agreement is poor. Under these conditions electrostatic repulsions are attenuated and any other soft interactions will come into play. But soft repulsions of any kind should depress the density of the I-N transition, as well as the density of the N-S transition. The poorer agreement between theory and experiment for the N-S transition seems more consistent with the known tendency of the cell model to overestimate the densities for positional ordering [1].

As mentioned in the Introduction, surfactant systems typically have a narrow or absent region of nematic stability [6,7]. With increasing density, cylindrical micelles typically make a transition directly from an isotropic to a hexagonal (columnar) phase. It is evident here (see Figs. 3 and 4) that soft repulsions can suppress the nematic phase. We would like to suggest that a qualitatively similar effect may account for the lack of an observed nematic phase in many surfactant systems. Micelles are flexible and often charged, so soft repulsions will be important for micellar phase diagrams. The extent to which self-assembly might modify this conclusion is a topic for future investigation.

ACKNOWLEDGMENTS

This work was supported by NIH Grants HL36546 and NRSA GM18932. We thank Donald J. Olbris for computer support.

[1] M. Taylor, R. Hentschke, and J. Herzfeld, Phys. Rev. Lett. **62**, 800 (1989).
[2] R. Hentschke, M. Taylor, and J. Herzfeld, Phys. Rev. A **40**, 1678 (1989).
[3] A. Stroobants, H. Lekkerkerker, and D. Frenkel, Phys. Rev. A **36**, 2929 (1987).
[4] B. Mulder, Phys. Rev. A **35**, 3095 (1987).
[5] X. Wen and R. B. Meyer, Phys. Rev. Lett. **59**, 1325 (1987).
[6] N. Boden, P. H. Jackson, and K. McMullen, Chem. Phys. Lett. **65**, 476 (1979).
[7] N. Boden, S. Corne, and K. Jolley, J. Phys. Chem. **91**, 4092 (1987).
[8] J. Han and J. Herzfeld, in *Statistical Mechanics in Physics and Biology*, edited by D. Wirtz and T. C. Halsey, MRS Symposia Proceedings No. 463 (Materials Research Society, Pittsburgh, 1997), p. 135.
[9] E. Kramer and J. Herzfeld, J. Chem. Phys. **110**, 8825 (1999).
[10] H. Graf, H. Lowen, and M. Schmidt, Prog. Colloid Polym. Sci. **104**, 177 (1997).
[11] H. Graf and H. Lowen, Phys. Rev. E **59**, 1932 (1999).
[12] E. Kramer and J. Herzfeld (unpublished).
[13] W. H. Press, B. P. Flannery, S. A. Teukolsky, and W. T. Vetterling, *Numerical Recipes* (Cambridge University Press, Cambridge, 1989).
[14] J. R. Philip and R. A. Wooding, J. Chem. Phys. **52**, 953 (1970).
[15] G. S. Manning, J. Chem. Phys. **51**, 924 (1969).
[16] R. Podgornik and V. A. Parsegian, Phys. Rev. Lett. **80**, 1560 (1998); B.-Y. Ha and A. J. Liu, *ibid.* **81** (1998); F. J. Solis and M. Olvera de la Cruz, Phys. Rev. E **60**, 4496 (1999); B. I. Shklovskii, Phys. Rev. Lett. **82**, 3268 (1999).
[17] S. Fraden, in *Observation, Prediction, and Simulation of Phase Transitions in Complex Fluids*, edited by M. Baus *et al.*(Kluwer, Dordrecht, 1995), p. 113.
[18] M. A. Cotter and D. C. Wacker, Phys. Rev. A **18**, 2669 (1978).
[19] J. Tang and S. Fraden, Liq. Cryst. **19**, 459 (1995).
[20] Z. Dogic and S. Fraden, Phys. Rev. Lett. **78**, 2417 (1997).
[21] S. Chandrasekhar, *Liquid Crystals* (Cambridge University Press, Cambridge, 1977).
[22] X. Wen, R. B. Meyer, and D. L. D. Caspar, Phys. Rev. Lett. **63**, 2760 (1989).
[23] M. Hirai, S. Arai, T. Takizawa, Y. Yabuki, and Y. Sano, Phys.

Rev. B **55**, 3490 (1997).
[24] S. Fraden, G. Maret, and D. L. D. Caspar, Phys. Rev. E **48**, 2816 (1993).
[25] Th. Kirchhoff, H. Lowen, and R. Klein, Phys. Rev. E **53**, 5011 (1996).
[26] G. Oster, J. Gen. Physiol. **33**, 445 (1950).
[27] H. Boedtker and N. S. Simmons, J. Am. Chem. Soc. **80**, 2550 (1958).
[28] U. T. Reinhardt, E. L. M. de Groot, G. G. Fuller, and W.-M. Kulicke, Macromol. Chem. Phys. **196**, 63 (1995).
[29] J. D. Bernal and I. Fankuchen, J. Gen. Physiol. **25**, 111 (1941).